Optimal Ankle Compliance Regulation for Humanoid Balancing Control

Mohamad Mosadeghzad, Zhibin Li, Nikos G. Tsagarakis, Gustavo A. Medrano-Cerda,
Houman Dallali, and Darwin G. Caldwell

Abstract— Keeping balance is the main concern for humanoids in standing and walking tasks. This paper endeavors to acquire optimal ankle stabilization methods for humanoids with passive and active compliance and explain ankle balancing strategy from the compliance regulation perspective. Unlike classical stiff humanoids, the compliant ones can control both impedance and position during task operation. Optimal compliance regulation is resolved to maximize the stability of the humanoids. The linearized model is proposed to obtain the optimal ankle impedance for stabilizing against impacts. The nonlinear model is proposed as well and compared with the linear one. The proposed methods are validated by experiments on an intrinsically compliant humanoid using passivity based admittance and impedance controllers both in joint and Cartesian space.

I. INTRODUCTION

During operation in an unstructured workspace the highest priority for a humanoid is to keep its balance while standing on one or two feet. The relatively high center of mass position and the small sized feet make postural balancing, subject to external disturbances, not a trivial task.

Three types of balancing strategies are well known for humans [1] [2], [3] which are namely: ankle, ankle-hip and stepping strategies who use these skills in an individual or combined manner depending on the disturbance. Similar methods have been utilized in humanoids. Regulation of ground contact force distribution via torque control for balancing purposes has been used in [4], [5] and applied to Sarcos robot and also [6] implemented on the biped developed at DLR. All these robots are equipped with decentralized torque controllers allowing the active regulation of Cartesian Impedance. In [7] modulation of distributed contact forces to maximize the robot stability can be explained as a desired Cartesian impedance. Regulation of impedance during balancing is also evident in humans [8]. The effect of foot impedance, particularly how the ankle stiffness affects robots stability has been also studied during walking [9]. In addition, it has also been explored for improving the energy efficiency during walking [10]. It is well known that passive elasticity can absorb impacts and reduce contact forces with no time delay response. The work in [11] explores the use of

Mohamad Mosadeghzad is with the Department of Advanced Robotics, Istituto Italiano di Tecnologia, via Morego 30, 16163 Genova, Italy. and Faculty of Engineering, University of Genoa.
Email: mohamad.mosadeghzad@iit.it mmzad83.basu@gmail.com
Zhibin Li, Nikos G. Tsagarakis, Gustavo A. Medrano-Cerda, Houman Dallali and Darwin G. Caldwell are with the Department of Advanced Robotics, Istituto Italiano di Tecnologia, via Morego 30, 16163 Genova, Italy.
Email: (zhibin.li, nikos.tsagarakis, Gustavo.Cerda, houman.dallali, darwin.caldwell)@iit.it
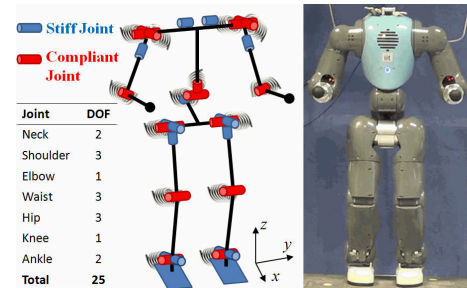
Fig. 1. Full body CoMan and its kinematics model

passive elastic elements for improving the robot stability and tried to identify suitable range of passive stiffness to achieve this goal.

These works show the effective regulation of the foot impedance has a significant effect on postural control. In most of the above cases the impedance parameters was experimentally tunned. However, selection of the impedance reference is still an open question. Emerging variable impedance actuation technology demands for suitable compliance profiles. As a response to this need several works explored optimal control policies to derive effective impedance trajectories for various tasks such as throwing or kicking where achieving the maximum velocity at ultimate time was used as the performance index [12] [13]. The contribution of this paper is to provide insights on how to generate effective ankle impedance profiles for the humanoid balancing problem using optimal control strategies. It is shown that for a range of impacts even a fixed value of passive stiffness in ankle can be adequate for optimal balancing performance. The optimal value of ankle impedance is derived analytically and numerically based on different cost functions in both linear and nonlinear models to minimize the center of pressure and mass deviation. This optimal value is used in the ankle balancing strategy on the **Co**mpliant Hu**Man**oid CoMan robot [14]–[16] (see Fig. 1). Theoretical results are verified by experiment and simulation [17]. Furthermore, the condition which ankle strategy fails is also discussed.

The paper is organized as follows. Section II introduces CoMan humanoid and its model. Section III elaborates the compliant ankle strategy while section IV presents experimental results. We conclude the study in section V.

II. COMAN HUMANOID MODELING

In this work we use the one degree of freedom (DOF) inverted pendulum model with the mass m and moment of inertia I_c around the COM, as shown in Fig. 2 to model CoMan humanoid platform [14] which its lower body is used

TABLE I
PARAMETERS BASED ON LOWER BODY OF COMAN

|	
m:	mass of the lower body; $16.5\,Kg$
I_c:	inertia tensor around the COM; $\simeq 0.9537\,Kgm^2$
I:	inertia tensor around the ankle pivot; $I = I_c + ml^2$
l:	nominal pendulum length from the COM to the pivot; $34\,cm$
θ:	desired angular position of ankle
q:	angular position of the link
K_a, D_a:	ankle stiffness/damping of active impedance
K_p:	ankle stiffness constant of passive spring; $400\,\frac{Nm}{rad}$
D_p:	ankle passive damping constant; $\simeq 2.5\,\frac{Nm\cdot s}{rad}$
K, D:	resultant stiffness/damping of the COM around ankle
d_1:	upper limit of x_{cop} based on the robot foot size; $11.5\,cm$
d_2:	lower limit of x_{cop} based on the robot foot size; $4.5\,cm$
ξ:	damping ratio of the ankle impedance
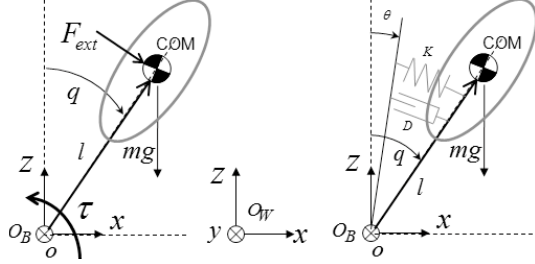
Fig. 2. Schematic model of the linearized inverted pendulum. Left: Free body diagram of the robot in sagittal plane; Right: Ankle torque represented by compliance.

for the experimental validation. In Fig. 2, the origin of the local reference frame O_B is located in the midpoint of right and left foot local reference frames. The origins of these coordinate systems are placed in the projection of the ankles pitch and roll intersection points to the ground. Frame O_B coincides with inertial coordinate O_W on the ground if feet stay in full contact with the ground.

In this model q represents the pendulum angle while F_{ext} is the sagittal disturbance which can be an impact or a constant force applied perpendicularly to the pendulum. Finally, τ denotes the torque around the ankle. The effective stiffness K and damping D of the model at the center of mass level is the result of the combined passive K_p, D_p and active K_a, D_a stiffness and damping in joint space. By applying $\sum(\tau_o) = I\ddot{q}$ we can now derive the dynamic equation of motion:

$$-\tau + l \cdot F_{ext} + mgl\,sin(q) = (I_c + ml^2)\ddot{q}. \quad (1)$$

The parameters used in the modeling and formulas in this paper are defined in Table I. The center of pressure of robot, x_{cop}, is:

$$x_{cop} = \frac{\tau}{m(g + \ddot{z})}, \quad (2)$$

where $z = lcos(q)$ is the center of mass height.

III. COMPLIANT ANKLE STRATEGY

A. Optimal Constant Compliance- Linearized Model

The dynamic equation of motion (1) is linearized around $q = 0$ assuming that the sagittal range of motion is confined to $-10° < q < 10°$. Taking into account that $\int_0^\epsilon F_{ext}dt = m\dot{q}_0$, where $\dot{q}_0$ is the initial velocity, the impact force in (1) can be considered as an initial COM velocity as a result of the impact . ϵ the ideal impact time $\to 0^+$. Considering

$u = \tau$ as the control input $x_1 = q$ and $x_2 = \dot{q}$ as the system states (1) can be written in state space form as follows:

$$\begin{cases} \dot{x} & = Ax + Bu, \\ A & = \begin{pmatrix} 0 & 1 \\ \frac{mgl}{I} & 0 \end{pmatrix}, B = \begin{pmatrix} 0 \\ -\frac{1}{I} \end{pmatrix}, \\ x_1(0) & = 0, \dot{x}_1(\infty) = 0, x_2(0) = v_0, \dot{x}_2(\infty) = 0, \end{cases} \quad (3)$$

where $I = I_c + ml^2$ is the moment of inertia around pivot point. K and D are the resultant torsional stiffness and damping respectively due to the series active impedance controller and the passive elasticity. Therefore $K = \frac{K_a K_p}{K_a + K_p}$ with the upper bound of the total stiffness being limited by the level of passive stiffness K_p. In addition, in the linearized model the position of the COP x_{cop} in (2) can be approximated by $\frac{\tau}{mg}$. The $\ddot{z}$ term has minor effect on the x_{cop}. Since x_{cop} inside the convex polygon is sufficient condition for whole body stability, an optimization cost function can be defined as:

$$J_1 = \int_0^\infty x^2{}_{cop}dt = \int_0^\infty \frac{\tau^2}{(mg)^2}\,dt = \int_0^\infty \frac{u^2}{(mg)^2}\,dt. \quad (4)$$

J_1 reduces the problem to a standard minimum effort Linear Quadratic Regulator (LQR) problem resulting in the algebraic Riccati equations and control input which is linear feedback of the states [18].

$$\begin{cases} -Q - A^T K_r - K_r A + K_r B R^{-1} B^T K_r = 0, \\ u = -R^{-1} B^T K_r x = \frac{(mg)^2}{I}(K_{r12}x_1 + K_{r22}x_2), \end{cases} \quad (5)$$

where $Q = \mathbf{0}$ and $R = \frac{1}{(mg)^2}$. K_r is the Riccati matrix which is symmetric with three independent elements K_{r11}, K_{r12} and K_{r22}. This matrix must be positive semidefinite to ensure a stable system. Solving the Riccati equations gives the optimal value of overall stiffness and damping which is the resultant of both active and passive impedance:

$$K_{r12} = \frac{2I \cdot l}{mg}, \qquad K_{r22} = \frac{2I}{mg}\sqrt{\frac{I \cdot l}{mg}}. \quad (6)$$

This feedback design can be implemented by a real physical compliance like a series elastic actuator (SEA) or a variable elastic actuator (VSA). The ankle torque will be:

$$\tau = K(q - \theta) + D\dot{q}, \quad (7)$$

where θ is the free length of spring and is considered constant $\theta = 0$. In analogy to torsional stiffness and damping equation (7), the optimal stiffness and damping can be derived from (6) with minimal x_{cop} deviation:

$$K = 2mgl, \qquad D = 2mg\sqrt{\frac{I \cdot l}{mg}}. \quad (8)$$

Therefore, the optimal stiffness and damping are constant as a function of the physical properties of the robot. The value of K is twice the minimum value of stiffness, mgl, which ensures asymptotic stability for the robot, $mgl < K \leq K_p$. This level of optimum stiffness can be interpreted as follows. The normal pendulum creates torque around the pivot which originates from the gravity torque, $mglq$. To achieve the same stabilizing effect with the inverted pendulum a spring that generates equivalent torque of $mglq$ when perturbed from the equilibrium is required. In the case of the inverted pendulum model the spring should generate
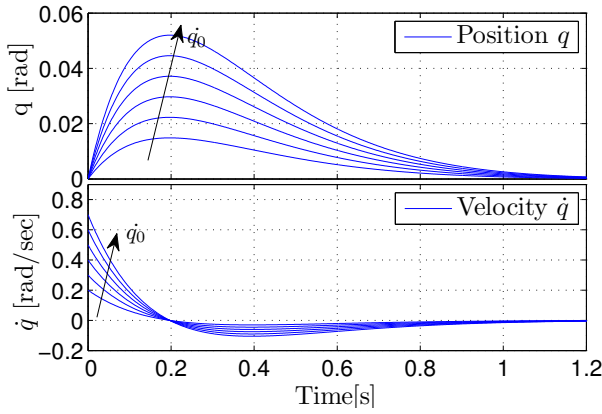
Fig. 3. Position, $q[rad]$ and velocity, $\dot{q}[rad/s]$ of ankle sagittal joint due to initial velocities from 0.2 to $0.7rad/sec$ by incremental of $0.1rad/sec$
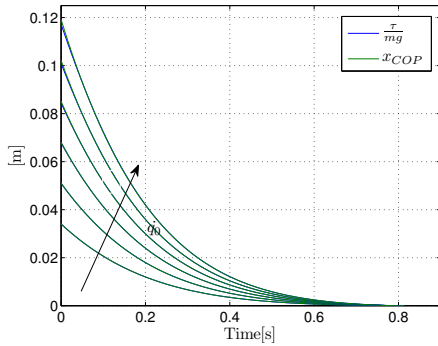

Fig. 4. x_{cop} and τ/mg deviation of robot after impact due to initial velocities from 0.2 to $0.7rad/sec$ by incremental of $0.1rad/sec$

additional torque to counterbalance the gravity torque $mglq$. In overall, a spring with stiffness of $2mgl$ as in (8) is required to stabilize the inverted pendulum similar to normal pendulum.

The natural frequency of the inverted pendulum system with the constant optimal value of stiffness (8) is $\omega_n = \sqrt{\frac{mgl}{I}}$. Accordingly $\frac{D}{I} = 2\xi\omega_n$ which results in a critically damped system with $\xi = 1$. The ξ is damping ratio of second order vibration systems, $0 \leq \xi < \infty$.

Simulation results for different initial COM velocities using the optimal stiffness and damping values given by (8) are presented in Fig. 3 and Fig. 4. The position and velocity of ankle sagittal joint are plotted in Fig. 3.

Since in static case, the projection of the center of mass on the ground should be inside the foot polygon, introducing a penalty on the ankle deflection q might also be considered. Another cost function can be formulated as follow:

$$J_2 = \int_0^\infty (x_{cop}^2 + \delta x_{com}^2)\mathrm{d}t, \qquad (9)$$

where the δ denotes the center of mass deviation weight. The x_{cop} has basically static and dynamic part. To understand this concept, center of pressure is derived using (1) and (2) as a function of q, $\dot{q}$ and $\ddot{q}$:

$$x_{cop} = \frac{mgl\sin(q) - I\ddot{q}}{m(g - l\ddot{q}\sin(q) - l\dot{q}^2\cos(q))}. \qquad (10)$$

This equation can be linearized around the upright position assuming that $q\ddot{q} \simeq 0$. The x_{cop} can be substituted by the linearized form of (10). Substituting (10) into (9), yields:

$$J_2 \simeq \int_0^\infty ((1 + \delta)(lq)^2 + (\frac{I}{mg})^2\ddot{q}^2)\,\mathrm{d}t. \qquad (11)$$

The COM projection to the ground, x_{com} is the position component of the x_{cop} which is lq. Therefore, $\delta > 0$ in (9) and (11) can be explained as giving more weight to the position deviation reduction of center of pressure. Also $\delta < 0$ will give more weight to the acceleration term of J_2. The δ can not be less than -1 which can cause a negative optimal cost function. Equation (9) will gives rise to the Q and R in the algebraic Riccati equations (5) equal to:

$$Q = \begin{pmatrix} \delta l^2 & 0 \\ 0 & 0 \end{pmatrix}, \qquad R = \frac{1}{(mg)^2}. \qquad (12)$$

Solving (5) using (12) yields:

$$K_{r12} = \frac{Il(1+\sqrt{1+\delta})}{mg}, \qquad K_{r22} = \frac{I\sqrt{2K_{r12}}}{mg}. \qquad (13)$$

The general formula for the optimal stiffness, damping and damping ratio in this case by using (5), (7) and (13) are:

$$\begin{cases} K = mgl(1 + \sqrt{1 + \delta}), \\ D = mg\sqrt{2\frac{I \cdot l(1+\sqrt{1+\delta})}{mg}}, \\ \xi = \frac{\sqrt{(2(1+\sqrt{1+\delta}))}}{2\sqrt{\sqrt{1+\delta}}}. \end{cases} \qquad (14)$$

This suggests that introducing the penalty on COM, $\delta > 0$ which is equivalent to giving more favor to the position component of COP reduction in (11) results in larger stiffness and damping than $\delta = 0$ or $\xi = 1$. Introducing a positive δ implies to an under damped systems with $\xi < 1$. It was predictable since giving more weight to the position part of COP in (11) will get more freedom to the transient dynamics. The under damped systems has more dynamic transient freedom than over damped ones. $\lim_{\delta\to\infty} \xi = \frac{\sqrt{2}}{2}$. It is the minimum damping ratio which only consider the position component of x_{cop} reduction and leads to a stable system. If only the x_{com} deviation as a static approximation of x_{cop} is considered then the limit of the center of mass will be:

$$-sin^{-1}(d_2/l) < q < sin^{-1}(d_1/l). \qquad (15)$$

On the other hand, $\delta < 0$ results in $\xi > 1$ which implies to over damped systems and causes less stiffness and damping than the critical damped system ($\xi = 1$). In these systems the proportion of transient dynamics is less than under damped systems. Therefore, giving more weight to acceleration of COP in (11) minimize the dynamic movements. The pure static motion can be reached by killing the acceleration part of COP while $\lim_{\delta\to-1} \xi = \infty$. In this case $\lim_{\xi\to\infty} K = mgl$. The $\xi = 1$ gives shortest settling time. Consider $\delta = -1$ in (11) then the cost is the minimization of the functional $\ddot{q}^2$. The optimal control for this problem does not stabilize the system but produces a zero cost when the initial velocity is zero and the initial position is not zero. In this case the system remains in static equilibrium since the controller produces torque to counteract the gravity. For zero initial position and nonzero velocity, the optimal control will not produce a zero cost, although it will drive the system to zero velocity and acceleration, the position will be left at

a nonzero value. Therefore, the controller will bring COM to a static equilibrium over time. However the closed loop system is still not stable because there is a zero eigenvalue.

B. Variable Optimal Compliance-Linearized Model

So far, for small impacts, no limits are placed on the control input and states since x_{cop} stays inside the feet polygon. However, this is not the case for large impact forces. Considering the foot size and boundary positions d_1 and $-d_2$ and the fact that x_{cop} should be always inside the foot polygon the following limits for the ankle torque can be derived $-d_2 < \frac{\tau}{mg} < d_1$ or $-mgd_2 < u < mgd_1$. According to minimum Pontryagin principle [18], the optimal input u^*, regardless of the optimization cost function (J_1 or J_2) and any values of δ, is:

$$\begin{cases} u^* = mgd_1 & u > mgd_1, \\ u^* = u & -mgd_2 < u < mgd_1, \\ u^* = -mgd_2 & u < -mgd_2. \end{cases} \quad (16)$$

Considering (16), $max(\dot{q}_0) = \frac{mgd_1}{D}$. This is derived from (7) for zero q and θ. If the optimal damping D from (8) is used, maximum initial velocity will be $max(\dot{q}_0) \simeq 0.74 rad/sec$. This initial velocity causes the maximum x_{com} deviation of $q = 3.83°$ which is in the limit (15). Initial velocities larger than $max(\dot{q}_0)$ will simply force the x_{cop} to the boundary causing the robot to tip over around edge.

The optimal controller is a state feedback scheme which can be implemented by the stiffness and damping gains K and D respectively as shown in (7). Therefore, it becomes clear that the initial jump of x_{cop} as seen in Fig. 3 is because of the torque generated by the damping component due to initial velocity $\dot{q}_0$ while the COM position at the beginning is zero the spring component does not produce any torque. By including the x_{cop} regulation in the optimal control problem the damping gain can be decreased during time to prevent exceeding the torque limits and keep the x_{cop} within the support polygon. As the natural frequency of the linearized inverted pendulum is $\sqrt{\frac{K-mgl}{I}}$ therefore, stiffness and damping are related as:

$$D = 2\xi I \sqrt{\frac{K - mgl}{I}}. \quad (17)$$

For high impacts it is necessary to regulate control gains online based on q and $\dot{q}$ according to (16). From (17) first K is obtained which gives the second equation in (18) and then substituting K in (7) for $\theta = 0$ gives the first equation in (18)

$$\frac{q}{4\xi^2 I}D^2 + \dot{q}D + mglq = \tau_{max}, \quad K = \frac{D^2}{4\xi^2 I} + mgl, \quad (18)$$

where τ_{max} is equal to either mgd_1 or $-mgd_2$ as in (16). For applying the control law (16) ξ is assumed to be constant before and after control signal reaches to its limit. When the input reaches to the extremum torques, impedance values using (18) will vary depending on q and $\dot{q}$ and this is what called *variable optimal compliance*. Equation (18) creates a varying gains feedback control because stability criteria for
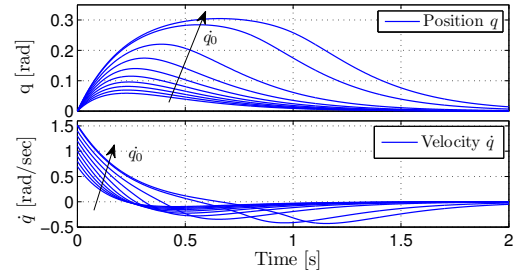

Fig. 5. Position, $q[rad]$ and velocity, $\dot{q}[rad/s]$ of ankle sagittal joint due to high impacts equivalent to initial velocities from 0.7 to 1.5rad/sec by incremental of 0.1rad/sec
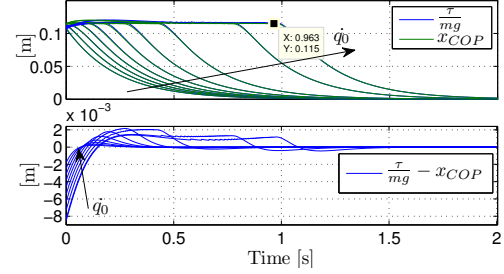

Fig. 6. x_{cop} and τ/mg deviation of robot after impact due to initial velocities from 0.7 to 1.5rad/sec by incremental of 0.1rad/sec

the constant feedback is not valid for linear time varying systems. Since the first equation of (18) has two solutions always the closet to the previous one should be chosen. Equation (17) indicates that stiffness can not be set bellow mgl and damping less than zero.

Fig. 5 to Fig. 7 present simulation results for $0.7 < \dot{q}_0 < 1.5$. The fixed optimal values were computed from (16) for $\delta = 0$ resulting $\xi = 1$. Regulation of compliance was then implemented on the basis of (18). Fig. 6 shows that difference between x_{cop} and τ/mg becomes bigger for large ankle angles however τ/mg is still a good approximation of x_{cop}. Also this figure indicates that using (18) the x_{cop} can be maintained within its limits of $d_1 = 11.5cm$. Fig. 7 illustrates that the largest initial velocity that the system can cope is $1.52rad/sec$ which leads to the minimum possible stiffness, mgl. The larger the initial velocity the bigger deviation of stiffness and damping from its constant value in (8). For the maximum initial velocity $\dot{q}_0 = 1.52rad/sec$, the ankle stiffness has to be decreased significantly resulting in the longest settling time. Fig. 5 shows that the maximum initial velocity can deviate ankle to $19.52°$ within the limit of (15), $-7.6° < q < 19.77°$.

C. Optimal Compliance- Nonlinear Model

Based on Fig. 5, $\dot{q}_0 > 1.2$ will lead the linear system to nonlinear regions. Also there are different kinds of external forces like smooth force or constant pushes which will increase the ankle deflection making the linear model invalid. For a wide range of disturbances a more general nonlinear model shall be considered. To do so the (1) and (2) are used. The new cost function in this case will be:

$$J_3 = \int_0^\infty x_{cop}^2 dt = \int_0^\infty \frac{\tau^2}{(mg + m\ddot{z})^2} \, dt, \quad (19)$$
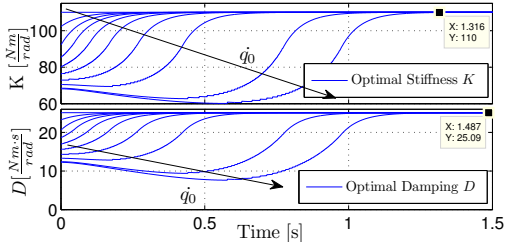
Fig. 7. Stiffness and damping variations for high impacts which cause x_{cop} jump to border of foot polygon. Initial velocities from 0.7 to $1.5\, rad/sec$ by incremental of $0.1\, rad/sec$

where $\ddot{z} = -l\left(\frac{lmg}{I}sin^2(x_1) - \frac{u}{I}sin(x_1) + \frac{l \cdot F_{ext}}{I}sin(x_1) + x_2{}^2 cos(x_1)\right)$. The objective is to minimize the Hamiltonian function:

$$\mathcal{H} = \frac{u^2}{(mg + m\ddot{z})^2} + \lambda_1 \dot{x_1} + \lambda_2 \dot{x_2}, \qquad (20)$$

where λ_1, λ_2 are costate variables. To minimize $\mathcal{H}$ for an unbounded optimal problem it is enough to solve:

$$\begin{cases} \dot{x}_1 = x_2, \\ \dot{x}_2 = \frac{mglsin(x_1)}{I} - \frac{u}{I} + \frac{l \cdot F_{ext}}{I}, \\ \frac{\partial \mathcal{H}}{\partial x_1} = -\dot{\lambda}_1 = \frac{Au^2}{(mg+m\ddot{z})^3} + \lambda_2\frac{mglcos(x_1)}{I}, \\ \frac{\partial \mathcal{H}}{\partial x_2} = -\dot{\lambda}_2 = \frac{4mlx_2u^2cos(x_1)}{(mg+m\ddot{z})^3} + \lambda_1, \end{cases} \qquad (21)$$

where $A = 2ml\left(\frac{2lmg}{I}cos(x_1)sin(x_1) + \left(-\frac{u}{I} + \frac{l \cdot F_{ext}}{I}\right)cos(x_1) - x_2^2sin(x_1)\right)$. The initial condition for solving these system of differential equations are $x_1(0) = 0, x_2(0) = 0, \lambda_1(\infty) = 0, \lambda_2(\infty) = 0$. Equation (21) can be solved by numerical integration.

Equations (21) and (22) should be solved numerically as a set of simultaneous differential and algebraic equations to compute control input, u^* while the input is not saturated otherwise (16) should be considered.

$$\frac{\partial \mathcal{H}}{\partial u} = 0 = \frac{2u(mg+m\ddot{z}) - (\frac{2ml}{I}sin(x_1))u^2}{(mg+m\ddot{z})^3} - \frac{\lambda_2}{I}. \qquad (22)$$

Fig. 8 shows the solution of (21) while the control limit (16) is considered. In this plot only the solution for $\dot{q}_0 = 1.3$ is depicted and the difference between the linear and nonlinear model is shown. It indicates that even for the large impacts the linear model and the proposed variable stiffness and damping method is enough for this type of disturbance. It justifies that (18) and (8) can be used instead of solving nonlinear equations for impacts.

However, the final solution for the control signal depends on F_{ext}. Equation (8) can only be used for impacts. This suggests that the optimal ankle torque for other types of disturbances should be derived by solving (21).

IV. EXPERIMENT

The parameters of CoMan lower body are listed in Table I. Two types of compliance regulators based on impedance [19] and admittance [20] schemes are available in the robot. The stiffness of the passive compliant joints are 520, 420, $390\, Nm/rad$ respectively for ankle, knee and hip. Experiments were performed only on the lower body of the robot. Stabilization by ankle compliance under range of impacts have done.
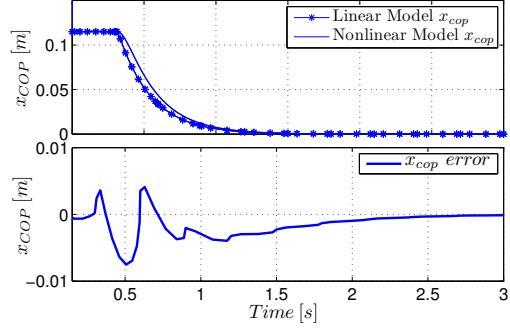

Fig. 8. Up: x_{cop} after impact due to initial velocity of $1.3\, rad/sec$ for linear and nonlinear model. Down: then difference between the x_{cop} of linear model with variable ankle impedance (18) and the nonlinear model (21)
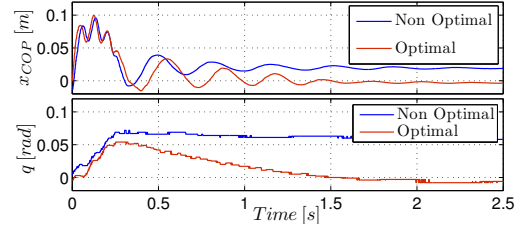

Fig. 10. Comparison of experimental results of constant stiffness and damping for optimal ($K = 2mgl$ $\xi = 1$ $\delta = 0$) and non optimal ($K = 1.27mgl$ $\xi = 1.528$) case and impact equivalent roughly to initial velocity of $0.7\, rad/sec$.

To apply a repeatable impact, a $5\, Kg$ weight suspended by a rope from a fixed frame is released from a specified height and collides with the wooden beam mounted on the waist of the robot. The x_{cop} and q deviation due to impact equivalent to $\dot{q}_0 = 0.7$ is shown in Fig. 10. The value of ankle optimal impedance is constant, $K = 110.0682\, Nm/rad$ and $D = 25.0964\, Nm \cdot s/rad$ based on (8).

It is clear from Fig. 10 that x_{cop} approaches to the limit $11.5\, cm$ and it decrease quickly after the impact for the optimal case. For instant a non optimal case is depicted in this plot. It is the over damped case ($K = 1.27mgl$ $\xi = 1.528$) and it is obvious that settling time is much larger than optimal one. The real impact in practice is not same as ideal impulse. For that reason the x_{cop} rises in a very short time and then decreases quickly while in the ideal case the x_{cop} jumps suddenly due to impact. Fig. 11 shows the large impact experiment which is equivalent to $\dot{q}_0 = 1.0$. The x_{cop} rises to the limit and fluctuates near the limit since the ankle compliance is variable based on (18). Then it decreases to the constant value according to (8) until the robot reaches the equilibrium. Fig. 12 plots the online update of stiffness and damping. The difference between this figure and Fig. 7 is due to the difference between real and ideal impact, inaccuracy in the modeling and responding delay of controller. The fluctuation of x_{cop} is due to the passive compliant elements in the waist of robot which are not controlled by admittance controller (see Fig. 10). However, the method is still effective and can maintain the balance of robot.

V. CONCLUSION

The optimal ankle's compliance of humanoids was found for low to high level of external impacts. It shows that
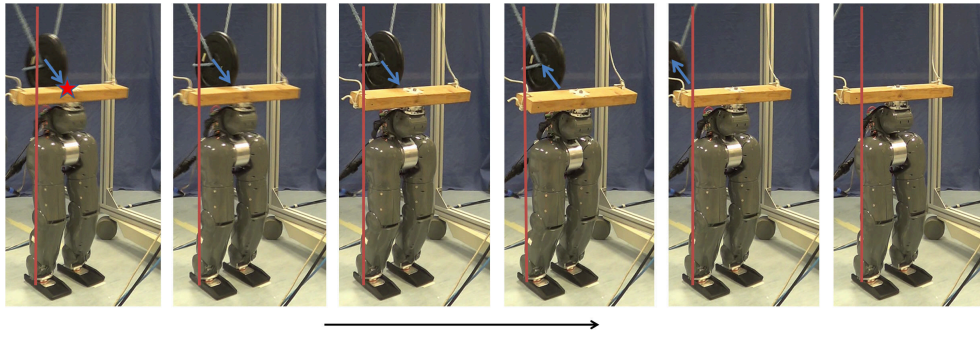
Fig. 9. Optimal compliance stabilizer (8) under impact experiment. The impact occurred in the first snapshot from the left.
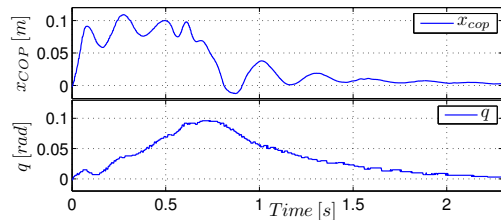

Fig. 11. Experimental results for variable stiffness and damping and impact equivalent roughly to initial velocity of $1.0\ rad/sec$ and $\xi = 1$.
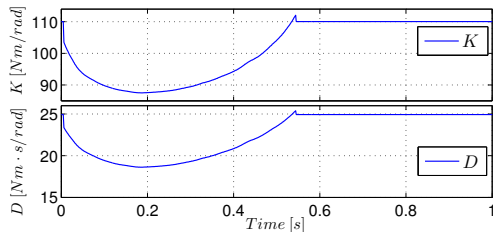

Fig. 12. Experimental results for variable stiffness and damping and impact equivalent roughly to initial velocity of $1.0\ rad/sec$ and $\xi = 1$.

optimal balancing torque can be generated by a passive or an active compliance regulator. The effect of introducing x_{cop} deviation in the cost function and its interpretation as a damping ratio ξ was addressed. A stabilization method was proposed to regulate the ankle compliance online for high level of impacts. The limitation of the ankle balancing strategy is determined. This is a criteria for ankle strategy failure which imposes the use of other balancing methods.

Acknowledgment

References

[1] A. Kuo, "An optimal control model for analyzing human postural balance," *IEEE Transactions on Biomedical Engineering*, vol. 42, no. 1, pp. 87–101, 1995.

[2] D. A. Winter, "Human balance and posture control during standing and walking," *Gait & Posture*, vol. 3, no. 4, pp. 193–214, 1995.

[3] F. B. Horak and L. M. Nashner, "Central programming of postural movements: adaptation to altered support-surface configurations," *Journal of Neurophysiology*, vol. 55, no. 6, pp. 1369–1381, 1986.

[4] B. Stephens and C. Atkeson, "Dynamic balance force control for compliant humanoid robots," in *IEEE/RSJ International Conference on Intelligent Robots and Systems*. IEEE, 2010, pp. 1248–1255.

[5] S.-H. Hyon, "Compliant terrain adaptation for biped humanoids without measuring ground surface and contact forces," *IEEE Transactions on Robotics*, vol. 25, no. 1, pp. 171–178, 2009.

[6] C. Ott, M. A. Roa, and G. Hirzinger, "Posture and balance control for biped robots based on contact force optimization," in *11th International Conference on Humanoid Robots*. IEEE-RAS, 2011, pp. 26–33.

[7] S. Hyon, J. Hale, and G. Cheng, "Full-body compliant human-humanoid interaction: Balancing in the presence of unknown external forces," *IEEE Transactions on Robotics*, vol. 23, no. 5, pp. 884–898, October 2007.

[8] P. G. Morasso and V. Sanguineti, "Ankle muscle stiffness alone cannot stabilize balance during quiet standing," *Journal of Neurophysiology*, vol. 88, no. 4, pp. 2157–2162, 2002.

[9] Y. Huang and Q. Wang, "Gait selection and transition of passivity-based bipeds with adaptable ankle stiffness," *Int J Adv Robotic Sy*, vol. 9, no. 99, 2012.

[10] R. Ghorbani and Q. Wu, "On improving bipedal walking energetics through adjusting the stiffness of elastic elements at the ankle joint," *International Journal of Humanoid Robotics*, vol. 6, no. 01, pp. 23–48, 2009.

[11] M.-S. KIM and H. O. JUN, "Posture control of a humanoid robot with a compliant ankle joint," *International Journal of Humanoid Robotics*, vol. 7, no. 01, pp. 5–29, 2010.

[12] M. Garabini, A. Passaglia, F. Belo, P. Salaris, and A. Bicchi, "Optimality principles in variable stiffness control: The vsa hammer," in *International Conference on Intelligent Robots and Systems*. IEEE/RSJ, 2011, pp. 3770–3775.

[13] S. Haddadin, M. Weis, S. Wolf, and A. Albu-Schäffer, "Optimal control for maximizing link velocity of robotic variable stiffness joints," in *IFAC World Congress*, 2011.

[14] N. Tsagarakis, S. Morfey, G. Medrano-Cerda, Z. Li, and D. G. Caldwell, "Compliant humanoid coman: Optimal joint stiffness tuning for modal frequency control," in *IEEE International Conference on Robotics and Automation*, Karlsruhe, Germany, 2013.

[15] N. G. Tsagarakis, Z. Li, J. Saglia, and D. G. Caldwell, "The design of the lower body of the compliant humanoid robot ccub," in *International Conference on Robotics and Automation*. IEEE, 2011, pp. 2035–2040.

[16] Z. Li, B. Vanderborght, N. G. Tsagarakis, L. Colasanto, and D. G. Caldwell, "Stabilization for the compliant humanoid robot coman exploiting intrinsic and controlled compliance," in *International Conference on Robotics and Automation*. IEEE, 2012, pp. 2000–2006.

[17] H. Dallali, M. Mosadeghzad, G. Medrano-Cerda, N. Docquier, P. Kormushev, N. Tsagarakis, Z. Li, and D. Caldwel, "Development of a dynamic simulator for a compliant humanoid robot based on a symbolic multibody approach," in *International Conference on Mechatronics*. IEEE, 2013.

[18] D. E. Kirk, *Optimal control theory: an introduction*. Dover Publications, 2004.

[19] M. Mosadeghzad, G. Medrano-Cerda, J. Saglia, N. G. Tsagarakis, and D. Caldwell, "Comparison of various active impedance control approaches, modeling, implementation, passivity, stability and trade-offs," in *International Conference on Advanced Intelligent Mechatronics*. IEEE/ASME, 2012, pp. 342–348.

[20] Z. Li, N. Tsagarakis, and D. G. Caldwell, "A passivity based admittance control for stabilizing the compliant humanoid coman," in *IEEE-RAS International Conference on Humanoid Robots*. IEEE, 2012, pp. 44–49.